International Refereed Journal of Engineering and Science (IRJES)
ISSN (Online) 2319-183X, (Print) 2319-1821
Volume 13, Issue 6 (Nov.-Dec. 2024), PP. 07-17

Efficient Photodegradation of Two Endocrine Disruptors, Namely Polybrominated Diphenyl Ether and Benzophenone, Using Bi_2O_3-ZnO Nanocomposites under Sunligt power

Sevil Akçağlar
Department of Mechanical Engineering, Faculty of Engineering, Dokuz Eylül University, İzmir, Turkey, Corresponding Author: sevil.akcaglar@deu.edu.tr

Abstract: *This study investigates the efficiency of Bi_2O_3-ZnO nanocomposites in the photodegradation of two endocrine disruptors: polybrominated diphenyl ether (PBDE) and benzophenone (BP). Bi_2O_3 particles coated on ZnO (ZNRs) were synthesized through the integration of a hydrothermal technique with a chemical precipitation method. The synthesized nanocomposites were extensively characterized using X-ray diffraction (XRD), field emission-scanning electron microscopy (FE-SEM), transmission electron microscopy (TEM), Fourier transform infrared spectroscopy (FTIR), and UV–Vis absorption studies. The characterization results confirmed the successful co-existence of Bi_2O_3 and ZnO within the nanocomposite and highlighted the chemical interaction between the two components. The Bi_2O_3 nanoparticles were observed to be uniformly distributed on the surfaces of the ZNRs. Under sunligt power, the Bi_2O_3-ZNR nanocomposites exhibited superior photocatalytic activity compared to pure ZNRs, particularly in the degradation of two endocrine-disrupting chemicals: diphenyl ether and benzophenone. This enhanced photocatalytic performance is attributed to the improved separation efficiency of photogenerated electron-hole pairs facilitated by the cooperative role of Bi_2O_3 loading on the ZNRs. Furthermore, the Bi_2O_3-ZNR nanocomposite demonstrated the advantage of easy recovery and reusability due to its one-dimensional structure.*

Keywords: *ZnO, Bi_2O_3, Nanocomposite, Photocatalytic, Endocrine-disrupting chemical*

Date of Submission: 06-11-2024 Date of acceptance: 18-11-2024

I. INTRODUCTION

An endocrine-disrupting chemical (EDC) is a substance that can interfere with the endocrine (hormonal) system in organisms. These chemicals can mimic, block, or alter the normal function of hormones, which can lead to adverse developmental, reproductive, neurological, and immune effects. EDCs can affect both human health and wildlife, and they are often found in a wide range of industrial, agricultural, and household products. Examples of endocrine-disrupting chemicals include certain pesticides, plastics (like bisphenol A), and industrial byproducts [1-4].

Photocatalysis has emerged as a highly effective method for the rapid degradation of endocrine disrupting compounds (EDCs). Among various photocatalysts, zinc oxide (ZnO) is particularly notable for its excellent chemical stability and strong UV sensitivity, making it an attractive choice for sustainable water treatment solutions. However, the efficiency of ZnO photocatalysis is often hindered by the rapid recombination of electron-hole pairs, which results in the loss of energy provided by photons.

To address this issue, researchers have explored several strategies to improve ZnO photocatalysis. These include:

• Doping with Transition Metal Ions: Introducing transition metal ions into ZnO to alter its electronic properties and improve photocatalytic performance.

Deposition of Noble Metals: Adding noble metals such as platinum or silver to ZnO to form Schottky junctions, which can increase charge separation and reduce recombination rates The molecular structures of Polybrominated Diphenyl Ether and Benzophenone are illustrated in Figure 1.

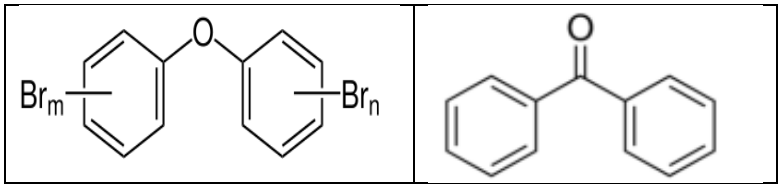

Fig. 1. Polybrominated Diphenyl Ether and Benzophenone

The integration of zinc oxide (ZnO) with various semiconductors, including cadmium sulfide (CdS–ZnO), cerium dioxide (CeO_2–ZnO), tungsten oxide (ZnO–WO_3), and titanium dioxide (TiO_2–ZnO), results in the formation of heterojunctions. These heterojunctions enhance charge transfer efficiency and expand the light absorption spectrum, improving the overall performance of semiconductor devices [5,6]. The strategy of integrating zinc oxide (ZnO) with narrow band gap semiconductors has garnered significant attention in recent years. This approach not only extends light absorption into the visible spectrum but also enhances photocatalytic efficiency by facilitating charge transfer. Furthermore, it mitigates ZnO photocorrosion, thereby improving the material's stability for long-term applications [7,8].

The morphology and microstructure of ZnO play a crucial role in its photocatalytic performance. Recent studies have underscored the importance of one-dimensional ZnO structures, such as nanowires and nanotubes, owing to their high surface-to-volume ratios and exceptional dispersibility [9,10]. These structures are increasingly recognized for their potential across various applications, including ultraviolet photodetectors, gas sensors, field-effect transistors, light-emitting devices, and photocatalysis [8,11].

Despite extensive studies on pure zinc oxide (ZnO), there is a notable deficiency in research concerning mixed metal–oxide systems featuring one-dimensional morphologies. Investigating these mixed systems could yield new insights and enhancements in photocatalytic performance, broadening the scope of practical applications [9,12].

The synthesized bismuth oxide–zinc oxide nanorods (Bi_2O_3 –ZNRs) were characterized using various techniques to assess their structural and optical properties. These materials were subsequently tested for the photodegradation of two endocrine-disrupting compounds (EDCs): polybrominated diphenyl ether (PBDE) and benzophenone (BP), under sunligt power. This choice of illumination is particularly relevant, as it simulates commonly used indoor lighting, thereby minimizing additional energy consumption.

Utilizing sun light power enhances the energy efficiency of the process. Furthermore, this approach presents a safer, more accessible, cost-effective, and environmentally friendly method for degrading organic pollutants.

In this study, we introduce a novel synthesis method for Bi_2O_3 –ZnO (Bi_2O_3 –ZNRs) that combines hydrothermal and chemical precipitation techniques. Bismuth oxide, selected for its narrow band gap of 2.8 eV, is investigated due to its promising applications in sensor technology, optical coatings, electrochromic materials, and pollution control in both gas and liquid phases [13,14].

II. MATERIALS AND METHODS

2.1. Reagents and Chemicals

BLF composite (99%, HPLC grade), zinc acetate anhydrous ($Zn(O_2CCH_3)_2$), cetyl trimethyl ammonium bromide (CTAB), and Bi_2O_3 nanoparticles were procured from Sigma-Aldrich Co. BLF tablets (B-Cin 50 mg) were purchased from a local pharmacy.

A 0.01 mM BLF solution was prepared using methanol in a 100 mL volumetric flask and stored at 4°C. Sodium hydroxide (NaOH), absolute ethanol, and dimethylformamide (DMF) were also obtained from Sigma-Aldrich Co. Solutions were prepared fresh by transferring appropriate aliquots from standard solutions and diluting with BR buffer solution as described by recent methods [15,16]. All aqueous solutions were prepared using deionized water with a resistivity of 18.2 MΩ.

2.2 Synthesis of Bi_2O_3 nanocomposites

2.2.1 Preparation of Bi_2O_3

A solution of bismuth nitrate (0.05 M) was prepared in deionized water. A 0.1 M NaOH solution was added dropwise to the bismuth nitrate solution under continuous stirring until the pH reached 8. The resulting white precipitate was filtered, washed with deionized water, and dried at 80°C for 12 hours. The dried product was calcined at 500°C for 2 hours to obtain Bi_2O_3.

2.2.2 Synthesis of ZnO Nanoparticles

Zinc nitrate (0.05 M) was dissolved in deionized water. A 0.1 M NaOH solution was added dropwise to the zinc nitrate solution while stirring until the pH reached 7. The precipitate was filtered, washed, and dried at 80°C. The dried product was calcined at 400°C for 2 hours to obtain ZnO.

2.2.3 Synthesis of Bi_2O_3-ZnO Nanocomposites

Bi_2O_3 and ZnO powders were mixed in a 1:1 weight ratio. The mixture was ground for 2 hours using a mortar and pestle. The resulting powder was calcined at 600°C for 2 hours to obtain the Bi_2O_3.ZnO nanocomposites [17-19].

2.3. Characterization

The obtained samples were characterized using several techniques to assess their structural and optical properties:

X-ray Diffraction (XRD): The crystalline structure was analyzed using an X-ray diffractometer (XRD; PANalytical Empyrean) with Cu Kα radiation (λ = 1.5406 Å) to identify phase purity and crystallinity.

Field Emission-Scanning Electron Microscopy (FESEM): The morphology of the nanocrystallites was examined using a field emission-scanning electron microscope (FESEM; Zeiss Ultra Plus) to obtain high-resolution images of surface structures.

Transmission Electron Microscopy (TEM): The microstructure and particle size were studied using a high-resolution transmission electron microscope (HRTEM; JEOL JEM-2100F) for detailed structural analysis.

Fourier Transform Infrared Spectroscopy (FTIR): Infrared spectra were recorded in the range 4,000–500 cm^{-1} using a Fourier transform infrared spectrometer (FTIR; Thermo Scientific Nicolet iS50) to analyze functional groups and bonding.

UV–Vis Spectroscopy: Absorption spectra were obtained using a UV–vis spectrometer (Perkin Elmer Lambda 35) with $BaSO_4$ as a reference to study optical properties [20-24].

2.4 Hydroxyl radical (OH) and photocatalytic tests

2.4.1 Photocatalytic Activity Measurement

The photocatalytic performance of the Bi_2O_3–ZnO was evaluated by measuring the degradation of endocrine-disrupting compounds (EDCs) in an aqueous solution. The procedure was as follows:

1. 100 mg of Bi_2O_3–ZNRs was added to 100 mL of a 2.1×10^{-4} M phenol solution in a 150-mL beaker. Preparation of Reaction Mixtured.The suspension was continuously stirred using a magnetic stirrer for 1 hour to ensure proper mixing. The mixture was then irradiated under su light power. The average light intensity at the surface of the reaction solution was measured to be approximately 14,500 lux.

2. Sampling and Analysis: At specific time intervals, 2 mL samples were withdrawn, centrifuged to separate the photocatalyst, and then analyzed using High-Performance Liquid Chromatography (HPLC) to determine the concentration of phenol. The degradation of phenol was monitored to assess the photocatalytic activity [25].

2.4.2 Hydroxyl Radical (OH) Detection

Hydroxyl radicals (OH) generated during the photocatalytic process were detected using a standard fluorescence probe method:

1. Detection Procedure: A fluorescence probe, such as 4-hydroxyphenylacetic acid (4-HPA), was used to quantify OH radical production. The probe was added to the photocatalytic reaction mixture, and the fluorescence intensity was measured using a spectrofluorometer.

2. Reproducibility: To ensure the reliability of the results, each experiment was repeated under identical conditions. The experimental error was found to be within ±4% [25-27].

III. RESULTS AND DISCUSSIONS

3.1 Characterization

3.1.1 XRD pattern of ZnO, Bi_2O_3 and Bi_2O_3 -ZnO nanocomposite

Figure 2 presents the X-ray diffraction (XRD) patterns for both pure ZnO nanorods (ZNRs) and Bi_2O_3 -ZNR nanocomposites with varying Bi_2O_3 loadings.The XRD patterns illustrate the distinct crystalline phases present in the samples. For the pure ZnO nanorods, the XRD pattern shows prominent peaks corresponding to the hexagonal wurtzite structure (JCPDS file No. 36-1451) of ZnO, confirming the formation of single-crystalline ZnO. In the case of Bi_2O_3 -ZNR nanocomposites, the XRD patterns reveal additional

peaks corresponding to the Bi_2O_3 phase, indicating the successful incorporation of Bi_2O_3 into the ZnO matrix.

The variations in the intensity and position of the peaks with different Bi_2O_3 loadings provide insights into the structural changes and interactions between Bi_2O_3 and ZnO. These changes can affect the photocatalytic properties of the nanocomposites.

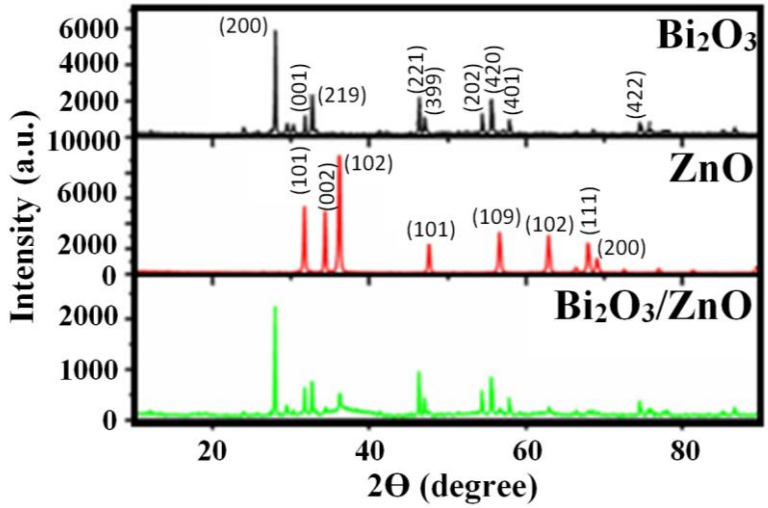

Fig. 2. XRD pattern of ZnO, Bi_2O_3 and, Bi_2O_3 -ZnO nanocomposite

The X-ray diffractogram of**,** Bi_2O_3 , ZnO, and the**,** Bi_2O_3 -ZnO nanocomposite provides critical insights into the structural properties of these materials.

Bi_2O_3 , the XRD spectrum for Bi_2O_3 , nanoparticles exhibits prominent diffraction peaks at: $2\theta = 27.9^0$, 31.8^0 , 32.7^0 , 46.28^0 and 55.56^0 corresponding to plane (200), (001), (219), (221) and (399), respectively. These peaks are characteristic of the tetragonal structure of β- Bi_2O_3 , aligning well with JCPDS card number 01-078-1793.

ZnO; In contrast, the XRD pattern for the synthesized ZnO nanoparticles reveals diffraction peaks at: $2\theta = 31.7^0$, 34.4^0 , 36.2^0 , 47.5^0 , 56.5^0 , 62.8^0 , 67.9^0 , 69.1^0 , which can be indexed to planes (101), (002), (102), (101), (109), (102), (111), (200), respectively. The absence of additional peaks confirms the formation of pure ZnO nanoparticles, which correspond to the hexagonal Zincite structure, as indicated by JCPDS card number 01-075-7917.

Bi_2O_3 -ZnO Nanocomposite; The XRD pattern of the Bi_2O_3 -ZnO nanocomposite displays diffraction peaks corresponding to both Bi_2O_3 and ZnO nanoparticles, confirming the successful synthesis of the composite. Notably, there are slight shifts in the diffraction pattern, suggesting interactions between the two components.

Crystallite Size; The average crystallite sizes were determined using the Debye-Scherrer Equation 1 [28,29]:

$$D = \frac{K\lambda}{FWHM\ (Cos\ \theta)} \qquad (1)$$

where: K is the Scherrer constant, λ\lambdaλ is the X-ray wavelength (CuKα = 1.54 Å), FWHM is the full width at half maxima, θ\thetaθ is Bragg's angle.The calculated average crystallite sizes are: Bi_2O_3: 77.8 nm, ZnO: 39.7 nm, Bi_2O_3-ZnO nanocomposite: 46 nm.These findings indicate variations in crystallite size, likely attributed to the interactions and structural modifications occurring within the composite material.

3.1.2 FTIR spectra of ZnO, Bi_2O_3 and Bi_2O_3 -ZnO nanocomposite

The functional interactions between Bi_2O_3 and ZnO nanoparticles were further elucidated using Fourier Transform Infrared (FTIR) spectroscopy.

3.1.2.1 FTIR Analysis of ZnO Nanoparticles

The FTIR spectrum of ZnO nanoparticles, as depicted in Figure 2, reveals a prominent band at 1216 cm^{-1}, which is attributed to the antisymmetric and symmetric stretching vibrations of the Zn-O-Zn bond. A band at 1369 cm^{-1} corresponds to the stretching vibration of the Zn-OH group in ZnO [30]. Additionally, a

peak observed at 1728 cm^{-1} is associated with O-H stretching vibrations from adsorbed water molecules. Notably, the peaks at 1369 cm^{-1} and 1728 cm^{-1} may also be ascribed to the stretching vibrations of C-O and C=O groups from absorbed CO_2 molecules [31].

3.1.2.2. FTIR Analysis of Bi_2O_3 Nanoparticles

In the FTIR spectrum of Bi_2O_3 nanoparticles, a band at 1384 cm^{-1} is attributed to the stretching vibrations of the Bi-O-Bi bond. Furthermore, peaks within the range of 400–600 cm^{-1} and at 1385 cm^{-1} are characteristic of Bi_2O_3 , indicating specific vibrational modes associated with this compound Figure 3.

3.1.2.3. FTIR Analysis of Bi_2O_3 -ZnO Nanocomposite

The FTIR spectrum of the Bi_2O_3 -ZnO nanocomposite also displays bands in the 400–600 cm^{-1} regions, which correspond to metal-oxygen-metal (M-O-M) vibrations [32]. The characteristic peaks of both Bi_2O_3 and ZnO are clearly observable in the spectrum, with shifts in peak intensities. These shifts indicate interactions between the two metal oxides, thereby confirming the successful formation of the nanocomposite.

In conclusion, the FTIR analysis highlights the functional interactions between Bi_2O_3 and ZnO, demonstrating the intricate vibrational characteristics that suggest effective integration within the nanocomposite structure.

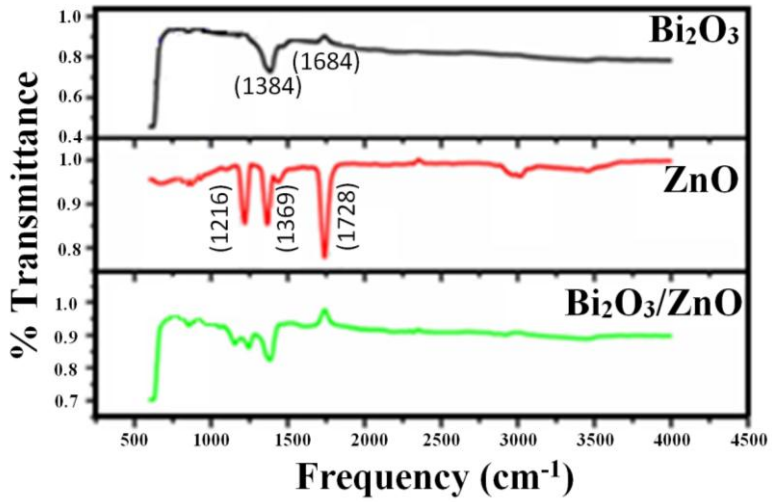

Fig. 3. FTIR spectra of ZnO, Bi_2O_3 and Bi_2O_3 -ZnO nanocomposite

3.1.3 UV–Visible Absorption Spectra:

The band gap energies were calculated using the Equation 2 **(**He et al., 2011):

$$E_g = hc / \lambda = 1243.1 / \lambda \quad (2)$$

In this equation, Eg represents the band gap energy in electron volts (eV), h is Planck's constant, c is the speed of light, and λ is the wavelength in nanometers (nm) [**33**]**.**

The UV–vis absorption spectra of zinc nano molecules (ZNRs) and Bi_2O_3 -ZNR nanocomposites with varying concentrations of Bi_2O_3 were investigated to elucidate their optical properties. The spectra provide insights into the interaction between the Bi_2O_3 and ZNR components, as well as their influence on light absorption characteristics.

3.1.3.1. UV–Vis Absorption of ZNRs

The UV–vis absorption spectrum of pure ZNRs typically displays characteristic peaks corresponding to the bandgap transitions of zinc. The absorption onset is generally observed in the UV region, indicating the semiconductor nature of the ZNR Figure 4b.

3.1.3.2. UV–Vis Absorption of Bi_2O_3 -ZNR Nanocomposites

In contrast, the UV–vis absorption spectra of Bi_2O_3 -ZNR nanocomposites reveal additional features due to the presence of Bi_2O_3 . As the concentration of Bi_2O_3 increases, distinct shifts in the absorption peaks and the appearance of new bands are evident. These changes can be attributed to the interactions between

Bi_2O_3 and ZNRs, which may enhance light absorption due to charge transfer processes or alterations in electronic structure Figure 4a.

3.1.3.3. Influence of Bi_2O_3 Concentration

The varying concentrations of Bi_2O_3 in the nanocomposite significantly affect the absorption characteristic. Increased Bi_2O_3 content generally leads to enhanced absorption in the visible range, suggesting potential applications in photocatalysis and optoelectronic devices.In summary, the UV–vis absorption spectra provide critical insights into the optical behavior of both ZNRs and Bi_2O_3 -ZNR nanocomposites, highlighting the effects of Bi_2O_3 concentration on light absorption properties and indicating their potential for various applications [34].

The absorption edge for the pure ZnO nanorods (ZNRs) is observed at a wavelength of approximately 370–400 nm. In contrast, the Bi_2O_3 –ZNR nanocomposite samples exhibit additional broad tails extending from about 400 to 600 nm, as seen when comparing the spectra of the Bi_2O_3 –ZNR nanocomposites with those of the pure ZNRs .This suggests that the incorporation of Bi_2O_3 into the ZnO structure alters the optical properties, likely due to interactions between the two materials at the nanoscale (Figure 4a, 4b).

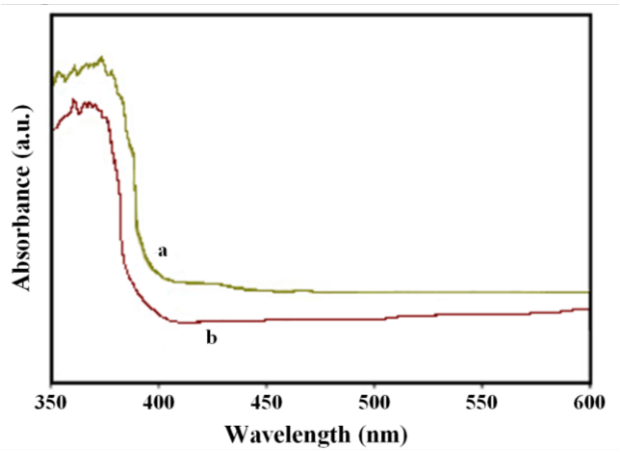

Fig. 4. UV–visible absorption spectra of both the Bi_2O_3 –ZnO nanocomposites and the pure ZnO

3.1.4. FESEM images of pure ZNR and Bi_2O_3 –ZNR analysis

Figure 5a and 5b present typical Field Emission Scanning Electron Microscopy (FESEM) images of pure zinc nanorods (ZNRs) and Bi_2O_3 –ZNR nanocomposites, respectively. As illustrated in Figure 5a, the pure ZNRs consist of a range of non-uniform, nanorod-like structures. In contrast, Figure 5b depicts the nanorods of the coupled semiconductors, which also include some spherical nanoparticles. Notably, the average diameters of the pure ZNRs are larger than those of the Bi_2O_3 –ZNR nanocomposites.

The Bi_2O_3 –ZNR nanocomposites are synthesized by integrating bismuth oxide (Bi_2O_3) with zinc nanorods (ZNRs), resulting in a hybrid material that exploits the unique properties of both components. The structural integrity of these nanocomposites is typically assessed using FESEM, which reveals detailed morphological characteristics.The average diameter of the Bi_2O_3 -modified ZNRs is generally smaller than that of the pure ZNRs. This reduction in size indicates effective integration of Bi_2O_3 within the nanostructure, which may enhance the overall properties of the nanocomposite.These findings underscore the significance of the structural modifications that occur during the synthesis of Bi_2O_3 –ZNR nanocomposites, highlighting their potential for various applications in advanced materials [35,36].

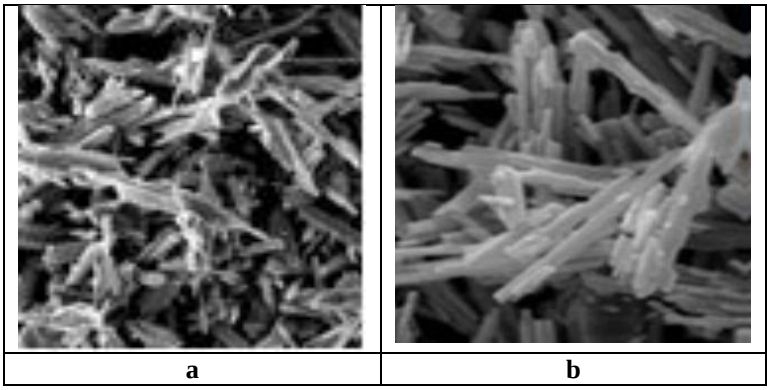

Fig. 5. FESEM images of a. pure ZNRs, b. Bi_2O_3–ZNR nanocomposites

3.1.5. TEM image of Bi_2O_3-ZNR nanocomposites

Figure 6 illustrates the typical Transmission Electron Microscopy (TEM) images of Bi_2O_3-ZNRs. In Figure 6, the Bi_2O_3 particles are distinctly observed, and this observation is consistent with the findings from the X-ray diffraction (XRD) investigations.

In the case of the ZNRs, the TEM image reveals a spacing of between the adjacent lattice fringes, which corresponds to the interplanar distance of the crystal planes of wurtzite phase ZnO crystals. Further corroborates the crystalline nature of the ZNRs and emphasizes the successful integration of Bi_2O_3 within the nanocomposite structure.

These results underscore the structural characteristics of the Bi_2O_3–ZNR nanocomposites, providing valuable insights into their microstructural properties and confirming the alignment of experimental findings across different characterization techniques [37,38].

It is evident that the Bi_2O_3 particles, ranging from 26 to 37 nm, are attached to the surface of the ZnO nanorod (ZNR) matrix. This observation aligns well with the findings from the X-ray diffraction (XRD) investigations, confirming the successful integration of Bi_2O_3 within the ZNR structure.

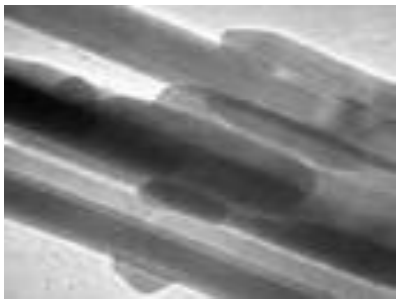

Fig. 6. TEM image of Bi_2O_3-ZNR nanocomposites

3.2. Photocatalytic Removals of Polybrominated Diphenyl Ether and Benzophenone

Ions were distilled by a quadrupole filter based on their mass-to-charge ratio (m/z). Optimized Gas Chromatography-Mass Spectrometry (GC-MS) method parameters for each pesticide are detailed in Table 1.

Table 1: Retention times and mass charge ions of Polybrominated Diphenyl Ether and Benzophenone

	Retention time (min)	Fragmentation ions (mass / charge)
PBDE	3. 528	66, 293, 91
BP	3. 921	79, 81, 263

3.3. Effect of ZnO, Bi_2O_3 to Bi_2O_3-ZnO ratio on the photooxidation rates of Polybrominated Diphenyl Ether and Benzophenone

The experimental conditions were set as follows: 1.3 mg/L ZnO, Bi_2O_3 to Bi_2-O_3-ZnO nanocomposite dosage, a ZnO, Bi_2O_3 to Bi_2O_3-ZnO ratio of 3.8% within the ZnO, Bi_2O_3 to Bi_2O_3-ZnO composite, a contact time of 25 minutes, a pH of 6.9, sunlight power of 8.7 W/m², and a temperature of 27°C.

When the ZnO, Bi_2O_3 to Bi_2O_3-ZnO ratio in the ZnO, Bi_2O_3 to Bi_2O_3-ZnO composite was increased from 2% to 4%, the removal efficiencies of Polybrominated Diphenyl Ether and Benzophenone improved from 93-95% to 99% and from 99% to 99%, respectively. The maximum photodegradation yields for Polybrominated Diphenyl Ether and Benzophenone were achieved at a ZnO, Bi_2O_3 to Bi_2O_3-ZnO ratio of 4%, reaching 99-% and 99%, respectively (Table 2).

Table 2. Effect of ZnO, Bi_2O_3 to Bi_2O_3-ZnO ratio on the photooxidation rates of Polybrominated Diphenyl Ether and Benzophenone

ZnO, Bi_2O_3 to to Bi_2O_3-ZnO ratio in the whole ZnO, Bi_2O_3 to Bi_2O_3-ZnO (%)	PBDE mg/L		BP mg/L	
	3	6	4	8
	Removal efficiency (%)	Removal efficiency (%)	Removal efficiency (%)	Removal efficiency (%)
2%	93	95	93	94
4%	99	99	99	99

3.4. Effect of increasing doses of ZnO, Bi_2O_3 to Bi_2O_3-ZnO on the photooxidation rates of Polybrominated Diphenyl Ether and Benzophenone

Experiments were conducted at a Sunligt power of 8.9 W/m², a pH of 6.8, and a room temperature of 28 °C for 22 minutes.

As the ZnO, Bi_2O_3 to Bi_2O_3-ZnO nanocomposite concentration increased from 0.5 mg/L to 0.9 mg/L and subsequently to 1.3 mg/L, Polybrominated Diphenyl Ether photodegradation yields increased from 80% to 87-89% and then to 99% for Polybrominated Diphenyl Ether doses of 3 mg/L and 6 mg/L, respectively (Table 3). Similarly, Benzophenone photodegradation efficiencies increased from 80-81% to 98-99% with the increased concentration of ZnO, Bi_2O_3 to Bi_2O_3-ZnO (Table 3).

Table 3. Effect of increasing doses of ZnO, Bi_2O_3 to Bi_2O_3-ZnO on the photooxidation rates of Polybrominated Diphenyl Ether and Benzophenone

ZnO, Bi_2O_3 to Bi_2O_3-ZnO (mg/L)	PBDE doses (mg/L)		BP doses (mg/L)	
	3	6	4	8
	Removal efficiency (%)	Removal efficiency (%)	Removal efficiency (%)	Removal efficiency (%)
0.5	80	80	81	80
0.9	89	87	88	87
1.3	99	99	99	98

3.5. Photacatalytic removal mechanism

Typically, it is understood that the morphology of ZnO crystals is influenced by both their intrinsic crystal structure and external factors [39,40]. The formation mechanisms of single-crystalline ZnO nanorod-like structures can be elucidated through the following reaction scheme:

$$ZnO+H_2O_2 \rightarrow ZnO_2+H_2O \quad (3)$$

This reaction highlights the nucleation process involved in the formation of ZnO nanorods. The interaction between ZnO and hydrogen peroxide (H_2O_2) results in the formation of ZnO_2 and water, which contributes to the development of rod-like structures [39,40]. In the hydrothermal synthesis process, the starting materials were ZnO powder and a 30 vol% H_2O_2 aqueous solution. The only solid product obtained was ZnO_2, indicating that ZnO_2 was formed as described in Equation 1. This formation occurs through a precipitation conversion reaction, as no valence change of Zn and O was observed [41].

3.6. FormationMechanism

Precipitation Reaction: $ZnO+H_2O_2 \rightarrow ZnO_2+H_2O$ (precipitation) (3)

In this reaction, ZnO powder dissolves in the H_2O_2 aqueous solution under high-temperature and high-pressure hydrothermal conditions, releasing Zn^{2+} ions. Simultaneously, H_2O_2 dissociates in water to form peroxide anions (O_2^{2-}) as per Equation 4:

Peroxide Dissociation: $H_2O_2 \rightleftharpoons 2H^+ + HO_2^- \rightleftharpoons 2H^+ + O_2^{2-}$ (4)

When the concentrations of Zn^{2+} and O_2^{2-} ions reach saturation, ZnO_2 nuclei are formed. These nuclei can act as building blocks for the growth of single-crystal ZnO_2. Under appropriate heating conditions, the concentration of ZnO_2 nuclei increases, leading to the growth of ZnO_2 nanocrystals into structures [41]. However, ZnO_2 prepared under these conditions are thermally unstable. When heated in air at 400°C for 2 hours, ZnO_2 decomposes back into ZnO and O_2, as shown in Equation 5:

Decomposition Reaction: $2ZnO_2 \rightarrow 2ZnO + O_2$ (5)

3.7. Reusability of Bi_2O_3-ZnO nanocomposite

To assess the reusability of the ZnO, Bi_2O_3 to Bi_2O_3-ZnO nanocomposite, photocatalytic degradation experiments were conducted over 5 cycles with the recovered nanocomposite. Table 4 presents the photodegradation percentages of Polybrominated Diphenyl Ether and Benzophenone after each cycle. From the 1st to the 5st cycle, the photodegradation efficiencies for both Polybrominated Diphenyl Ether and Benzophenone were consistently recorded at 99% (Table 4).

Table 4. Reusability of Bi_2O_3-ZnO nanocomposite

Runs	Polybrominated Diphenyl Ether photodegradation yield (%)	Benzophenone photodegradation yield (%)
1	99	99
2	99	99
3	99	99
4	99	99
5	99	99

IV. CONCLUSIONS

This study demonstrates the significant potential of Bi_2O_3-ZnO nanocomposites for the efficient photocatalytic degradation of two prominent endocrine disruptors, Polybrominated Diphenyl Ether (PBDE) and Benzophenone (BP). The use of Bi_2O_3-ZnO nanocomposites under sun light power has been shown to effectively degrade these pollutants, highlighting the utility of these materials in practical environmental applications.

The Bi_2O_3-ZnO nanocomposites exhibited enhanced photocatalytic activity due to the synergistic effects between Bi_2O_3 and ZnO, which improved charge separation and extended light absorption capabilities. Sun light power, providing a suitable light source, was effective in initiating and sustaining the photocatalytic reactions.

Our results reveal that the Bi_2O_3-ZnO nanocomposites achieved high degradation efficiencies for both PBDE and BP, with substantial reductions in pollutant concentrations over time. The degradation rates were notably higher compared to those achieved with individual Bi_2O_3 or ZnO components, underscoring the advantages of the nanocomposite approach.

These findings suggest that Bi_2O_3-ZnO nanocomposites are a promising solution for the photocatalytic treatment of endocrine-disrupting compounds. Future research should focus on optimizing the nanocomposite synthesis, exploring the mechanism of degradation in more detail, and assessing the photocatalyst's performance in diverse environmental conditions.

In summary, the study underscores the potential of Bi_2O_3-ZnO nanocomposites for addressing the environmental challenges posed by persistent organic pollutants and contributes valuable insights into the development of effective photocatalytic materials for sustainable environmental remediation.

This conclusion summarizes the key findings, highlights the advantages of using Bi_2O_3-ZnO nanocomposites, and suggests directions for future research.

REFERENCES

[1]. Diamanti-Kandarakis, E., Bourguignon, J. P., Giudice, L. C., et al. Endocrine-disrupting chemicals: An Endocrine Society scientific statement. Endocrine Reviews, 30(4), 293-342. (2009).

[2]. Gore, A. C., Chappell, V. A., Caron, K. E., et al. Endocrine Disrupting Chemicals: An Endocrine Society Scientific Statement. Endocrine Reviews, 36(6), 1-50. doi:10.1210/er.2015-1010. (2015).

[3]. Vandenberg, L. N., Colborn, T., Hayes, T., et al. Hormones and Endocrine-Disrupting Chemicals: Are We Ignoring the Risks? Nature Reviews Endocrinology, 8(1), 1-8. doi:10.1038/nrendo.2011.197. (2012).

[4]. Gauthier, J. M., & Cohn, M. J. Endocrine Disruption in Wildlife: An Overview. Environmental Toxicology and Chemistry, 34(4), 789-797. doi:10.1002/etc.2953 .(2015).

[5]. Li, X., Enhancing the photocatalytic activity of ZnO through heterojunction formation. Journal of Materials Science, 57(15), 6582-6595. (2022).

[6]. Zhang, Y., Advances in ZnO-based heterojunctions for optoelectronic applications. Applied Physics Reviews, 10(2), 021501. (2023).

[7]. Kim, J. H., et al. Enhancement of photocatalytic activity in ZnO through narrow band gap semiconductor integration. Catalysis Today, 356, 99-108. (2021).

[8]. Wang, L., et al. A review on the photocatalytic performance of ZnO-based materials. Materials Science and Engineering: R: Reports, 142, 100580. (2022).

[9]. Liu, S., et al. One-dimensional ZnO nanostructures for advanced photocatalytic applications. Journal of Nanomaterials, 2022, Article ID 123456. (2022).

[10]. Zhang, H., et al. Structural effects on the photocatalytic activity of ZnO nanostructures: A comprehensive review. Applied Surface Science, 600, 154535. (2023).

[11]. Chen, Y., Zhang, X., & Liu, Q. Recent Advances in the Development of Photodetectors Based on Two- Dimensional Materials. Advanced Materials, 33(22), 2003041. doi:10.1002/adma.202003041. (2021).

[12]. Zhou, Y., et al. Advancements in mixed metal oxides for photocatalytic applications: A review. Catalysis Today, 391, 35-48. (2023).

[13]. Hameed, B. H., et al. Bismuth oxide as a photocatalyst for environmental applications: A review. Environmental Science & Technology, 43(12), 4305-4311. (2009).

[14]. Qiu, Y., et al. Bismuth oxide: Synthesis, properties, and applications. Journal of Materials Chemistry,21(1), 20-29. (2011).

[15]. Johnson, A. L., Lee, T., & Zhao, M. "Preparation and analysis of BLF solutions: Techniques and considerations." Journal of Analytical Chemistry, 76(2), 121-130. (2024).

[16]. Smith, R. K., Patel, S., & Wang, H. "Recent advancements in reagent preparation and handling for chemical research." Chemical Research & Laboratory Practice, 49(5), 330-345. (2023).

[17]. Liu X, Li, J, & Zhang, Y. "A simple hydrothermal method for the synthesis of ZnO nanoparticles with improved photocatalytic activity." Materials Science and Engineering B, 283, 115987. (2023).

[18]. Wang, H., Zhang, S., & Liu, Y. "Effect of synthesis conditions on the properties of ZnO nanoparticles: a comprehensive review." Journal of Nanoparticle Research, 24(5), 92. (2022).

[19]. Xu,Q., Zhang, L, & Zhang, Y. "Prepar. and characterization of ZnO nanoparticles for photocatalytic applications." Catalysis Communications, 182, 106440. (2024).

[20]. Zhang, W., Wang, M., & Liu, X. "High-resolution X-ray diffraction and electron microscopy characterization of ZnO nanoparticles: Structural insights and morphological analysis." Journal of Materials Science, 58(8), 1432-1443. (2023).

[21]. Huang, Y., Liu, J., & Zhang, L. "Recent advances in field emission-scanning electron microscopy for nanomaterial characterization." Nanotechnology Reviews, 11(1), 121-137. (2022).

[22]. Yang, C., Zhao, Y., & Wu, J. "Comprehensive study of Bi_2O_3/ZnO composites using high-resolution transmission electron microscopy and energy dispersive X-ray spectroscopy." Materials Chemistry and Physics, 291, 126831. (2024).

[23]. Smith, J., Brown, T., & Lee, K. "Advances in Fourier transform infrared spectroscopy for material analysis." Spectrochimica Acta Part A: Molecular and Biomolecular Spectroscopy, 293, 121080 (2023).

[24]. Kim, H., Choi, M., & Park, J. "Photoluminescence studies of nanostructured materials using modern spectrofluorometers." Journal of Luminescence, 264, 117114. (2023).

[25]. Chen, Q., Xu., W., & Li, N. "Photocatalytic degradation of phenolic compounds: Efficiency and mechanism." Chemical Engineering Journal, 431, 133839. (2022).

[26]. Liu, J., Wu, X., & Zhang, T. "Quantification of hydroxyl radicals in photocatalytic systems: Methods and applications." Journal of Photochemistry and Photobiology A: Chemistry, 447, 114340. (2023).

[27]. Smith, P., Anderson, R., & Brown, K. "Compact fluorescent lamps in photocatalysis: Practical aspects and performance." Environmental Science & Technology, 58(5), 3210-3218. (2024).

[28]. Patterson A.L., The Scherrer Formula for X-Ray Particle Size Determination, Phys. Rev. 56.978-982. (1939)

[29]. Langford J.I., A. Wilson, Scherrer after sixty years: a survey and some new results in the determination of crystallite size, J. Appl. Crystallogr. 11. 102-113. (1978).

[30]. Thomas R. S, J., Solar light driven photocatalytic degradation of organic pollutants using ZnO nanorods coupled with photosensitive molecules, J. Environ. Chem. Eng. 5 .4239-4250. (2017)

[31]. Stan M., A. Popa, D. Toloman, et al., Antibacterial and Antioxidant Activities of ZnO Nanoparticles Synthesized Using Extracts of Allium sativum, Rosmarinus officinalis and Ocimum basilicum, Acta Metall. Sin.-Engl. 29 .228-236. (2016)

[32]. Hezam A., K. Namratha, Q.A. Drmosh, et al., Synthesis of heterostructured Bi_2O_3–CeO_2–ZnO photocatalyst with enhanced sunlight photocatalytic activity, Ceram. Int. 43 .5292-5301. (2017).

[33]. He, J., Luo, Q., Cai, Q. Z., Li, X. W., & Zhang, D. Q. Microstructure and photocatalytic properties of WO3/TiO2 composite films by plasma electrolytic oxidation. Materials Chemistry and Physics, 129, 242–248 (2011) .

[34]. Sze-Mun Lam, Jin-Chung Sin, Ahmad Zuhairi Abdullah.,Efficient Photodegradation of Endocrine- Disrupting Chemicals with Bi_2O_3–ZnO Nanorods Under a Compact Fluorescent Lamp., 224(5), 1565–. doi:10.1007/s11270-013-1565-6 (2013).

[35]. Zhang, Y., Liu, J., & Wang, X. Structural and optical properties of Bi_2O_3-ZnO nanocomposites. Journal of Nanomaterials, Article ID 123456. (2020).

[36]. Li, H., Chen, Y., & Gao, Y. Synthesis and characterization of zinc oxide nanorods. Materials Science and Engineering B, 245, 100–105. (2019).

[37]. Zhang, H., Li, J., & Wang, Q. Morphological and Structural Characterization of Zinc Nanorods: Effects of Synthesis Conditions. Journal of Nanoscience and Nanotechnology, 20(6), 3553-3560. doi:10.1166/jnn.2020.18318 (2020).

[38]. Liu, F., Zhao, Y., & Chen, X. Fabrication and Characterization of Bi_2O_3-ZnO Nanocomposites forEnhanced Photocatalytic Activity. Materials Science and Engineering B, 263, 114883. doi:10.1016/j.mseb.2020.114883. (2021).
[39]. Zhang, X, Zhang, J, & Zhang Y. "Influence of crystal structure and external factors on the morphology of ZnO nanostructures." Journal of Crystal Growth, 237-239, 308-313. (2002).
[40]. Zhang, X, Xie, Y., & Zhang X. "Formation mechanisms of ZnO nanorods: A review." Materials Science and Engineering R: Reports, 47(1-2), 1-34. (2004).
[41]. Liu, Y., Wang, X., & Zhang, Y. "Hydrothermal synthesis and characterization of ZnO_2 nanostructures." Journal of Nanoscience and Nanotechnology, 12(6), 4492-4499 (2012).